Evidence of fast neutron detection capability of the CLLB scintillation detector

Felix Pino[a,b], Matteo Polo[c], Jessica C. Delgado[a], Giorgia Mantovani[a], Sara Maria Carturan[a,b], Daniela Fabris[c], Davide Brunelli[d], Lucio Pancheri[d], Alberto Quaranta[d,e], Sandra Moretto[a,c]

[a] *Department of Physics and Astronomy "Galileo Galilei", University of Padova, Via Francesco Marzolo, 8, Padova, 35121, PD, Italy*
[b] *INFN-Laboratori Nazionali di Legnaro, Viale dell'Università, 2, Legnaro , 35020, PD, Italy*
[c] *INFN- Padova Section, Via Francesco Marzolo, 8, Padova, 35131, PD, Italy*
[d] *Department of Industrial Engineering, University of Trento, Via Sommarive, 9, Povo, 38123, TN, Italy*
[e] *INFN-TIFPA Section, Trento, Via Sommarive, 14, Povo, 38123, TN, Italy*

Abstract

For the first time we report the ability of the CLLB scintillator to detect and discriminate fast neutrons (2-10 MeV energy range) from gamma-rays and thermal neutrons, using a digital pulse shape discrimination technique. Firstly, we conducted measurements in single mode with an Am-Be source, unshielded and shielded, and we tagged a new cluster of events as the fast neutron-induced zone. The Figure of Merit obtained for the fast neutron/gamma discrimination was 1.1. Then, in order to better characterize these new cluster of events induced by fast neutrons, we conducted measurements in coincidence mode. We used a mono-energetic pulsed neutron source, at the Van de Graaff accelerator facility at the Legnaro National Laboratories (INFN-LNL, Legnaro-Italy), and also, a continuous neutron spectrum (using a ^{252}Cf source). Combining all experimental results with a Monte Carlo model of the CLLB detector, built using the GEANT4 tool kit, it was

possible to obtain the light output function of ^{7}Li ions in the CLLB crystal ($dL/dE = \kappa$; $\kappa = 0.36 \pm 0.02$). Moreover, the intrinsic fast neutron efficiency was modeled by Monte Carlo, obtaining similar values 1.5-2 % for neutrons between 2 MeV and 10 MeV. Finally, an application of this new feature, in the field of nuclear security and nuclear safeguards, is given.
Keywords: CLLB, Fast Neutron Detection, Digital Pulse Shape Discrimination

1. Introduction

In the last years the discovery of new inorganic scintillation materials, able to be sensitive to several kinds of radiations, opened new perspectives not only in nuclear research experiments, but also in the nuclear applications field. Among these, the Elpasolite scintillators, such as: CLYC (Cs_2LiYCl_6:Ce), CLLC ($Cs_2LiLaCl_6$:Ce), CLLB ($Cs_2LiLaBr_6$:Ce), CLLBC ($Cs_2LiLaBr_{6-x}Cl_x$:Ce), CNYC (Cs_2NaYCl_6), etc., are some of the most interesting materials. Most of them exhibit excellent performances in terms of energy resolution (< 5 % at $E_\gamma = 662$ keV, good for identification of gamma emitters), due to their high light output (> 20000 photons/MeV) and linearity, and thermal neutron detection capability (Smith et al., 2013; Liang and Smith, 2020; Pérez-Loureiro et al., 2021; Hawrami et al., 2016). Furthermore, very often they show an excellent thermal neutron/gamma-ray discrimination performance (Giaz et al., 2016b; Mesick et al., 2017).

The thermal neutron detection capability in these types of scintillators is due to the presence of ^{6}Li, and the associated neutron capture reaction ^{6}Li(n,t)α (Q = 4.78 MeV). The energy deposited by the reaction products

(triton and alpha) produces a well-defined distribution of events at a gamma-equivalent energy between 3.2 MeV and 3.5 MeV, depending on the specific type and volume of the Elpasolite crystal.

Those Elpasolite scintillators that contain Chlorine (Cl) in their composition exhibit a very interesting feature, which is the fast neutron detection capability, exploiting the reactions ^{35}Cl(n,p)^{35}S (Q = 0.62 MeV) and ^{35}Cl(n,α)^{32}P (Q = 0.94 MeV). The use of these reactions to perform fast neutron detection and also neutron spectroscopy, employing a CLYC-6 and CLYC-7 (^{6}Li and ^{7}Li enriched CLYC respectively) detectors, has been studied and reported by (D'Olympia et al., 2014; Giaz et al., 2016a; Ferrulli et al., 2022), obtaining good results. The estimated intrinsic neutron detection efficiency is around 1 % (Mentana et al., 2016).

Having one single scintillator with multiple radiation discrimination capability, i.e. gamma-rays, thermal neutrons and fast neutrons (performing pulse shape discrimination analysis of the signals) represents a great advantage in applications like nuclear safeguards, hand-held monitors, plasma diagnostics of fusion reactors, industry (well-logging), and also fundamental nuclear physics experiments. In addition to the CLYC detector, some hybrid solutions (composite detector) have been already studied in order to achieve triple discrimination (Cester et al., 2016; Shirwadkar et al., 2017). However, coupling different scintillators introduces some complexities from the point of view of the mechanics (assembly of the detector), acquisition and data analysis (signals can be very different, so the acquisition and processing algorithms could not work properly).

The fast neutron detection capability of the CLLB scintillation detector

has been studied. According to (Woolf et al., 2016; Qin et al., 2018), the (n,2n) reactions on ^{79}Br and ^{81}Br are the most promising mechanisms to exploit it. However, in this case, the fast neutron is detected by measuring gamma and beta emissions of the products (^{78}Br and ^{80}Br respectively) of the reactions. In this way, it is impossible to obtain a triple discrimination.

In this work we demonstrate the fast neutron detection capability of the CLLB scintillation detector, using another mechanism to obtain the triple discrimination. Recently, we reported the results related to its excellent performance in terms of gamma-ray and thermal neutron detection and discrimination (Pino et al., 2021). Now, in this work, we provide a strong evidence of its fast neutron detection capability based on the elastic scattering of the fast neutrons with the lithium nuclei (^{7}Li), present in the CLLB crystal composition. From the kinematics of the reaction, a neutron is able to transfer a maximum of 44 % of its kinetic energy to a ^{7}Li nucleus. So, if one considers a neutron energy range from 1 MeV to 10 MeV, it will be expected to have ^{7}Li ion recoils with energies up to 4.4 MeV. It is important to underline some considerations: the amount of natural Li (92.4 % ^{7}Li and 7.6 % ^{6}Li) in the CLLB composition (10 % mol) is considerable, the quenching of the light yield by light ions in inorganic scintillators is low (Martínez-Dávalos et al., 1997; Cazzaniga et al., 2016), the neutron elastic scattering cross section on Li (mostly on ^{7}Li) is nearly one order of magnitude greater than the ones for (n,p) and (n,α) reactions on ^{35}Cl, for neutrons with energies between 1 MeV and 10 MeV (see Fig. 1).

In the following, we show the ability of the CLLB scintillator to detect and discriminate (using a digital pulse shape discrimination technique) be-

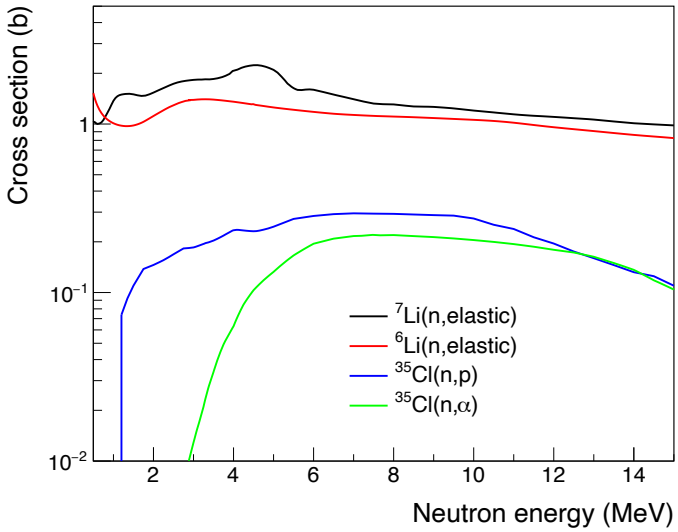

Figure 1: Neutron cross sections of relevant reactions for fast neutron detection. Data obtained using the NNDC ENDF database (ENDF/B-VII.1, http://www.nndc.bnl.gov, 2022.)

tween gamma-rays, thermal neutrons and also fast neutrons. By performing coincidence measurements, combined with Monte Carlo simulations, we are able to estimate the light output function of ^{7}Li ions in the CLLB crystal. Using the light output function it is possible to determine the intrinsic neutron efficiency in the 1-10 MeV energy range. Finally, we present an interesting application in the field of nuclear security and nuclear safeguards.

2. Experimental set-up

A 2"×2" cylindrical CLLB scintillation detector is used (Saint Gobain Crystals, https://www.crystals.saint-gobain.com/radiation-detection-scintillators/crystal-scintillators/cllb, last time seen on May 2022). The main physical properties

of this scintillator are: density 4.2 g/cm^3, light yield 40000 ph/MeV, hygroscopic, wavelength of maximum emission 420 nm. The scintillator is coupled to a 2" diameter Hamamatsu photomultiplier (PMT model R6231) using a Hamamatsu E1198-27-Y004 active voltage divider.

Bias voltage is applied using a CAEN V6533 VME HV Power Supply Module. A CAEN V2718 VME-PCI Optical Link Bridge is used to configure the HV power supply unit and the digitizer. A CAEN A3818 PCI Express CONET2 Controller installed on a PC is used to control the acquisition system (by means of optical fiber connections using the CAEN CONET2 protocol). The PMT signals are acquired by a CAEN V1730 fast digitizer (500 MSamples/s, 14-bit ADC resolution and Digital Constant Fraction Discriminator, DCFD, embedded in the firmware for precise timing measurements). The installed firmware (Digital Pulse Processing for Charge Integration and Pulse Shape Discrimination, DPP-PSD) can pre-process data determining the pulses timestamps and integrating them over two gates, in order to perform particle discrimination using the so-called double integration method (Pino et al., 2014). The ABCD (Acquisition and Broadcast of Collected Data) software, (Fontana et al., 2017, 2018, 2020), released as an open-source project[1]s used for data acquisition and electronic control.

In this work the pulse shape parameter (PSP) is computed as: PSP = Q_{short}/Q_{long}, where Q_{short} is the integral of the signal over a short window (w_1), including the fast rise time region and part of the fastest decay component of the pulse, and Q_{long} is the integral of the signal over a long window

[1] i

(w_2), encompassing the total pulse (used to estimate the energy deposited because it is proportional to the total light yield by the event). It is important to remark that using this convention it is expected to get larger PSP values for faster signals. The Figure of Merit (FoM), defined as $FoM = \Delta/(\delta_n+\delta_\gamma)$, was computed by analyzing the PSP distribution, where Δ is the difference between the two mean PSP values of the neutron and gamma PSP distributions and $\delta_n + \delta_\gamma$ is the sum of the Full Width at Half Maximum (FWHM) values (Cester et al., 2013).

As first, the energy calibration of our detector is done, using a set of gamma calibration sources (^{137}Cs, ^{22}Na, ^{60}Co, ^{133}Ba). Then, we perform measurements employing an Am-Be source (neutron emission rate $\sim 2 \times 10^5$ s^{-1}), which provided a combined neutron/gamma radiation field. The gamma sources are positioned in front of the detector face at 0.25 m. In single mode, the pulse shape analysis is the only way to discriminate between different incoming radiations. Indeed, coincidence measurements can provide further information to discriminate and recognize particles. For that reason we perform measurements in coincidence mode at the Van de Graaff accelerator at Legnaro National Laboratories (Legnaro, Italy) and using a ^{252}Cf source (with a continuous neutron spectrum, neutron emission rate at the time of the experiments $\sim 5 \times 10^4 \pm 20$ % s^{-1}). In Fig. 2 the experimental set-up used for the measurements at the accelerator facility is given. The mono-energetic neutrons are obtained by impinging a proton beam into a ^{7}LiF target (700 $\mu g/cm^2$ thick). The proton beam has a repetition rate of 3 MHz and a width of 2 ns, the proton beam energy is 5.5 MeV, thus the energy of the neutrons emitted at 0° is 3.8 MeV. The CLLB detector is

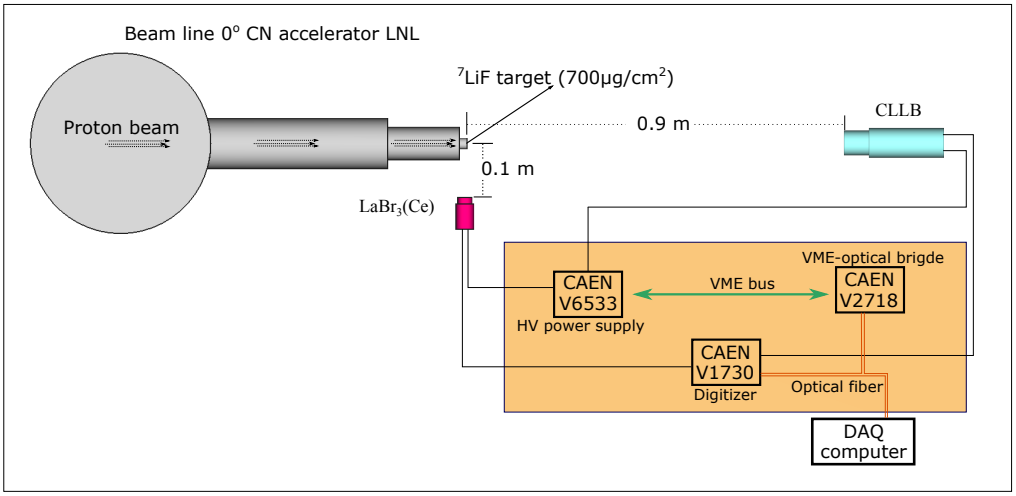

Figure 2: Experimental set-up at the CN accelerator facility (LNL, Italy).

placed in front of the ^{7}LiF target at a distance of 0.9 m. The coincidence events are tagged by measuring the gamma flash, produced by the protons impinging the target, with a 1" $LaBr_3$:Ce scintillation detector, positioned close to the target. Coincidences events are filtered on board by the CAEN V1730 digitizer. The experimental set-up using the ^{252}Cf source is similar to the one shown in Fig. 2. In this case, the ^{252}Cf replaces the ^{7}LiF target, and the events are tagged using the prompt fission gamma-rays ($\sim$ 9 gamma-rays per fission are emitted by the ^{252}Cf).

3. Results

3.1. Measurement in single mode using Am-Be

In Fig. 3a the 2D plot (pulse shape parameter versus the total light output in MeV electron equivalent) is presented, corresponding to the measurement using the Am-Be source moderated with 8 cm of polyethylene (four

blocks of 10 cm × 20 cm × 2 cm attached to the front-face of the detector). In this experimental condition, the gamma-ray and neutron capture on ^{6}Li induced events are easily recognized, as indicated in the figure. But, we recognize another cluster of events, populating an area having a low energy ($<$ 1 MeVee) and an average PSP value of 0.82. This PSP region corresponds to particles with higher stopping power (PSP values $\sim$ 0.8 are associated to alpha or alpha/tritium events from the intrinsic alpha background and neutron captures on ^{6}Li, respectively). By performing a test without the polyethylene moderator, see Fig. 3b the neutron capture cluster becomes less intense, as expected, because the thermal neutron field is strongly reduced, but the new cluster of events becomes more visible. It is important to note that the acquisition time in both measurements is the same. Taking into account that without the polyethylene moderator the neutron field consists mainly of fast neutrons (mean energy $\sim$ 4.2 MeV), we can ascribe the new events to fast neutron induced signals. Taking into account the events with light output lower than 1 MeVee, see Fig. 3c, we obtained a FoM = (1.1 $\pm$ 0.1) for fast neutron/gamma-ray discrimination. Considering that the Li content in the CLLB crystal is significant (10 % mol), the origin of the fast neutron events can be explained by the elastic scattering of the neutrons with the lithium nuclei (mostly ^{7}Li because the lithium in the CLLB crystal has natural abundance, i.e. 92.4 % ^{7}Li and 7.6 % ^{6}Li). Note that the maximum fraction of kinetic energy transferred from a neutron to a ^{7}Li nucleus is around 44 % (backscattering reaction). In order to further study the fast neutron events , in the next section we report the results of the measurements in coincidence mode.

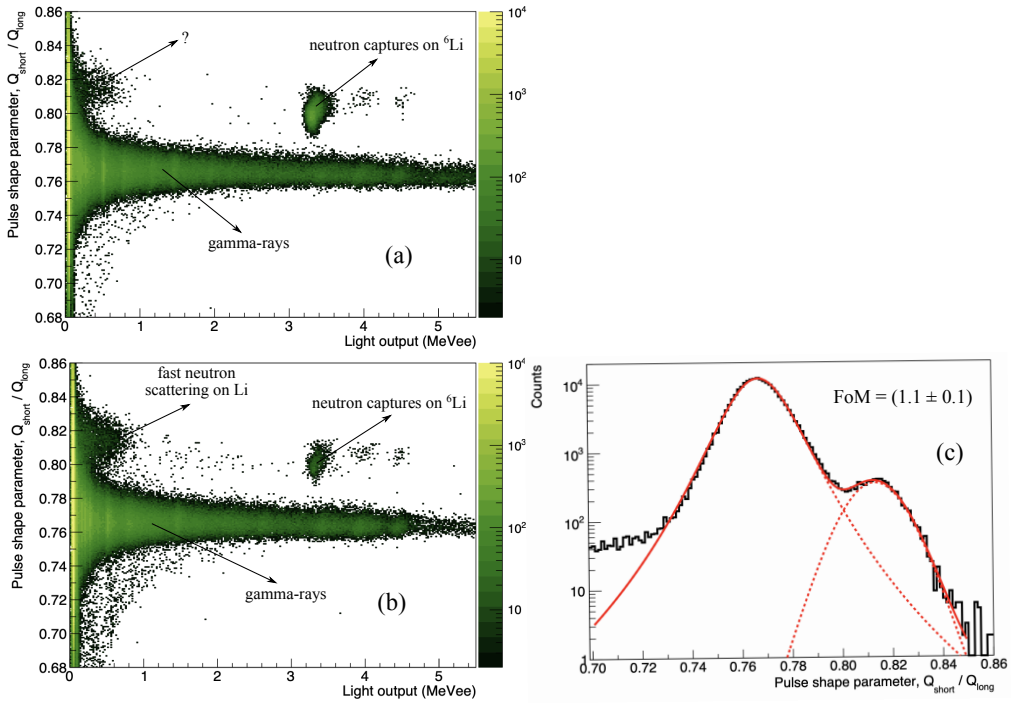

Figure 3: (a) 2D plot (pulse shape parameter against the light output) of the measurement using the Am-Be source moderated with 8 cm of polyethylene. (b) 2D plot using the Am-Be source nude. Both measurements lasted 10 minutes. (c) Pulse shape parameter distribution considering the events with light output values lower than 1 MeVee, FoM = (1.1 ± 0.1).

3.2. Measurement in coincidence mode

By performing coincidence measurements with the CLLB scintillation detector in a combined fast neutron/gamma-ray radiation field, it is possible to better recognize and discriminate the type of particle that induced the events. Fig. 4 reports the results obtained performing measurements with the ^{252}Cf source (first row), continuous fast neutron spectrum, and at the Van de Graaff accelerator facility (second row), with mono-energetic fast neutrons. Specifically, the 2D plots are given in Fig. 4a and 4d, respectively for the two experiment setups. Fig. 4b and 4e show the time of flight spectra considering only the events with PSP values greater than 0.793 (see dashed lines in Fig. 4a and 4d). As it can be seen, in both time of flight spectra the $\gamma - \gamma$ coincidence peak can be recognized (Δt $\sim$ 3 ns). As far as the neutron parts, in the case of the ^{252}Cf, a continuous γ-n coincidence distribution can be seen, while, in the case of the Van de Graaff measurements a γ-n coincidence peak is found (Δt = 33.4 ns, which corresponds to the time of flight of 3.8 MeV neutrons in 0.9 m flight path). The time resolution of the CLLB detector, σ_t = 1.9 ns, has been measured and reported in (Pino et al., 2021). Finally, Fig. 4c and 4f show the 2D plots considering only the events tagged as fast neutron induced events (γ-n coincidences in the range defined by the dashed lines in Fig. 4b and 4e). It is important to note that the selection in the time of flight spectrum of the measurement performed with the ^{252}Cf source includes neutrons from 1 to 10 MeV. As it can be observed, the position in the 2D plots of these events agrees with the hypothesis stated in the previous section. So, it has been successfully proved that this kind of events corresponds to fast neutrons interactions.

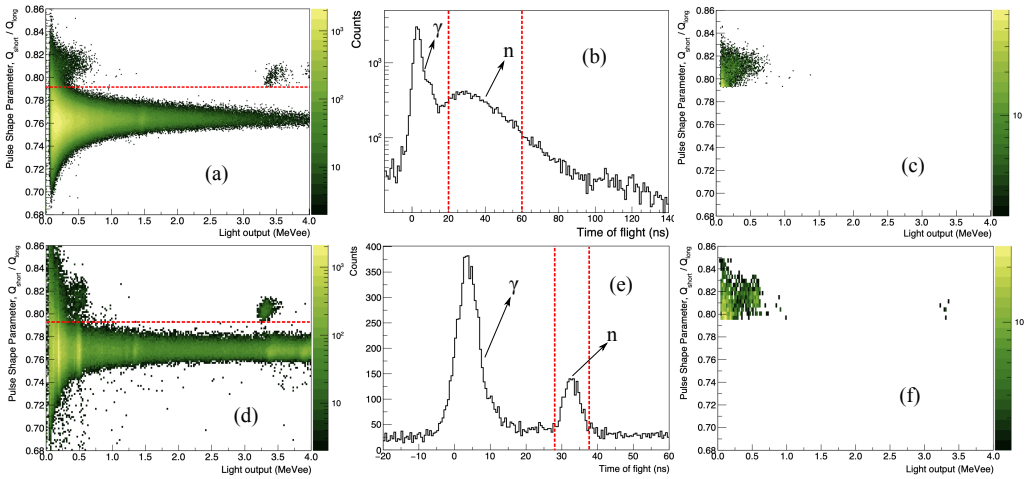

Figure 4: (a) 2D plot corresponding to the acquisition in coincidence mode with the ^{252}Cf, (b) time of flight spectrum of the events over the red dashed line on (a), (c) 2D plot of the events tagged as fast neutrons from the selection in (b). (d), (e) and (f) are similar than (a), (b) and (c) but with the measurements at the CN accelerator.

3.3. Monte Carlo simulations

In order to estimate the light output function associated to lithium ions and the intrinsic fast neutron detection efficiency of the CLLB scintillation detector, we perform Monte Carlo simulations using the toolkit Geant4 v10.7 (Allison et al., 2016). In the code, the neutrons are emitted at 0.9 m from the front face of the detector, and they are emitted in a cone towards the detector face. The initial energy of the neutrons is sampled from the well-known spontaneous fission neutron spectrum, in the case of the ^{252}Cf source (Al-Adili et al., 2020), or it is defined as a constant value (mono-energetic neutrons) for the experimental set-up of the Van de Graaff accelerator. A maximum of 10^7 primary neutrons are simulated during each run. The experimental set-up (detailed composition and geometry of the CLLB scintillation

detector, etc.) is reproduced in the G4VUserDetectorConstruction class. The neutron transport is managed with the high precision neutron model for low energy neutrons (< 20 MeV) included on the QGSP_BERT_HP physics list. With the use of the G4Step and G4Track classes (implemented on the G4UserSteppingAction class), it is possible to track the history of each event (primary and secondary particles) during each step, and for example, to access to the type of occured interaction , secondary particles created, kinetic energy of the particles, deposited energy in the volume of interest, etc.

3.3.1. Light output of lithium ions in the CLLB crystal

To determine the light output associated to lithium ions of the CLLB scintillation detector, the first step is to identify the creation of Li ions (both ^{6}Li and ^{7}Li) by means of elastic scattering of fast neutrons, and then, to save the kinetic energy of the recoil Li ions resulting after each neutron history. It is important to remark that more than one recoil Li ion can be created by only one neutron, so, these multiple scattering interactions are taken into account in our calculations. Once the simulation is done, the kinetic energies (in MeV) are converted into a light output (in MeVee), and taking into account that brilliant inorganic scintillators (such as elpasolite and halide scintillators) have very good light yield proportionality (Shirwadkar et al., 2011; Hull et al., 2019), the energy range of interest is not so wide (recoil Li ions from 0 to 4 MeV), and that similar inorganic scintillators show small deviations from linearity (Martínez-Dávalos et al., 1997; Cazzaniga et al., 2016; Dell'Aquila et al., 2019), the selected light output function is linear, i.e. $\frac{dL}{dE} = \kappa$. So, we are considering that the quenching effect is negligible in the examined energy range. $\frac{dL}{dE}$ is the amount of light produced per unit of energy released by the

Li ions in the CLLB crystal, and κ is known as the scintillation efficiency, that has been fitted by comparing the experimental and simulation results. In Fig. 5 the total kinetic energy distributions of the recoil ^{6}Li and ^{7}Li ions are reported for each case. The scintillation efficiency, κ, was optimized, and it was obtained $\kappa = (0.36 \pm 0.02)$. The comparison between the experimental and simulation results is given in Fig. 6b and 6c. As it can be observed, a good agreement between experimental and simulation results is obtained. The experimental data used for the comparison is obtained from Fig. 4c and 4f (projections over the light output axis of the 2D plots).

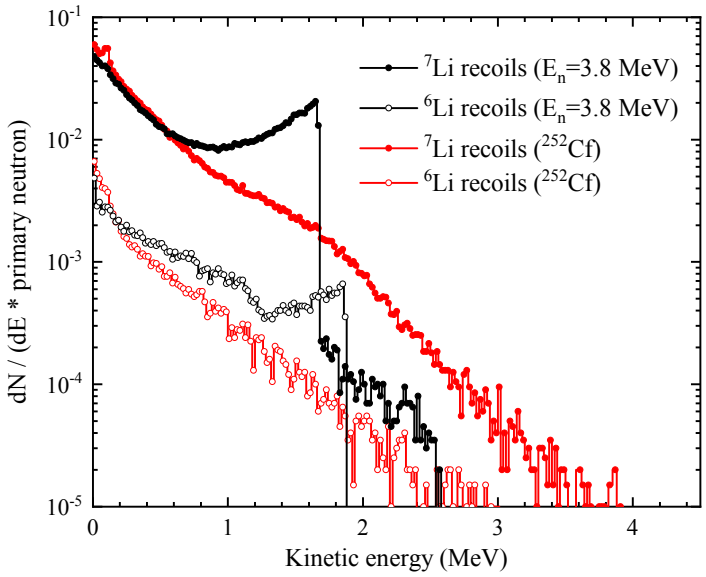

Figure 5: Monte Carlo simulations of the total kinetic energy of the Li ion recoils produced by a mono-energetic ($E_n = 3.8$ MeV) and a continuous neutron energy spectrum (^{252}Cf).

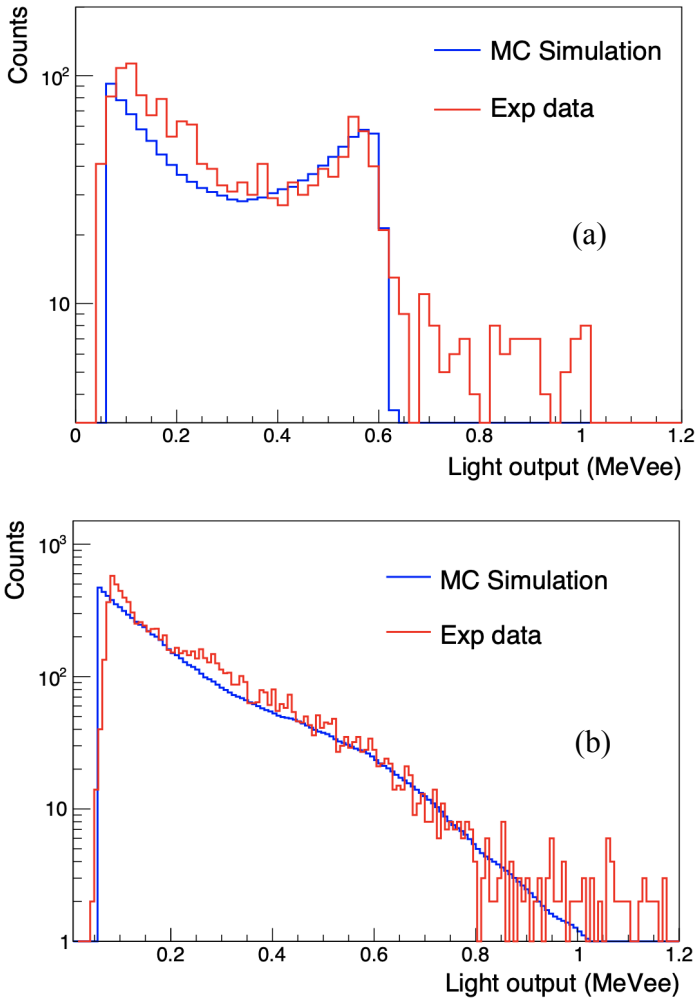

Figure 6: Comparison between simulation and experimental results using the data acquired using (a) mono-energetic neutrons (CN accelerator) and (b) the ^{252}Cf source.

3.3.2. Neutron detection efficiency

Using the light output function to Li ions reported in the previous section, it is possible to estimate the intrinsic neutron detection efficiency of the CLLB scintillation detector. In this case, mono-energetic neutrons are simulated from 1 MeV to 10 MeV in steps of 0.5 MeV. Some of the simulated responses (pulse height spectra) are given in Fig. 7a. By integrating these responses (over a determined threshold value), the intrinsic efficiency values can be obtained as a function of the energy of the incident neutron. The efficiency results are shown in Fig. 7b, having used a threshold value of 0.1 MeVee. The neutron efficiency starts to be significant (> 1 %) for neutrons with energy > 1 MeV, then, for neutrons with energy greater than 2 MeV, and up to 10 MeV, it shows a slight variation (between 1.5 and 2 %). It is important to note that the fast neutron efficiency exhibited by the CLLB scintillation detector exceeds by a factor of two the value reported for a CLYC-7 detector (fast neutron detection based on ^{35}Cl (n,p) and (n,α) reactions) (Mentana et al., 2016).

3.4. Application: source recognition

In order to illustrate the CLLB potential deployment in homeland security and nuclear safeguards applications, we perform a set of measurements with two different neutron sources, ^{252}Cf and Am-Be, shielded with several centimeters (from 0 to 8 cm) of polyethylene. As an example, Fig. 8a shows a 2D plot corresponding to the measurement with the ^{252}Cf source shielded with 4 cm of polyethylene. We can observe three cluster of events, identified and tagged as: gamma-ray, neutron captures or thermal neutrons and fast neutrons. We define the variable f as the ratio of neutron capture to fast

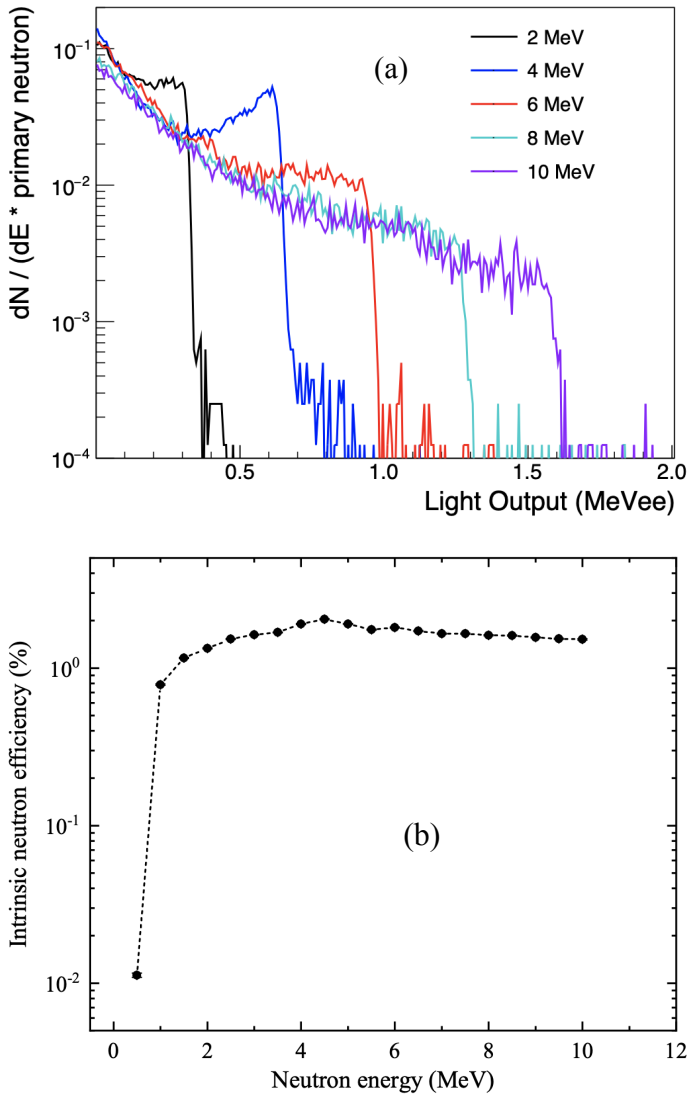

Figure 7: (a) Simulated responses (pulse height spectra) corresponding to mono-energetic neutrons of 2, 4, 6, 8 and 10 MeV. (b) Intrinsic neutron detection efficiency as a function of the energy of the incident neutron setting a threshold of 0.1 MeVee.

neutron counts ($f = N_{captures}/N_{fast}$). Looking at the correlation plot between f and the polyethylene thickness, we obtain the results shown in Fig. 8c. Both set of data show a linear behaviour ($y = a \cdot x + b$). The ordinates (b) are close to zero for both neutron sources, and the slope associated to the ^{252}Cf source is $\sim$ 7 times higher than the one corresponding to the Am-Be. It means that it is possible to recognize and estimate the thickness of the neutron source shielding using only the number of counts associated to neutron capture and fast neutron events, together with the well known gamma spectra ability. In our experimental test, the shielding is polyethylene, but these results can be easily extended to other shielding material.

In Fig. 8b gamma spectra, for ^{252}Cf and Am-Be, are shown, selecting only the events tagged as gamma events according to the previous definition of the zones in the 2D plot (see Fig. 8a). It can be seen that the two spectra show characteristics easily recognizable. In particular, the ^{252}Cf is a continuous and smooth spectrum (except from the 1.47 MeV peak associated to the internal background of the CLLB crystal, ^{138}La decay). The Am-Be gamma spectrum has two unique features: the gamma line at 4.44 MeV, coming from the de-excitation of the first state of ^{12}C, ^{9}Be(α,n)^{12}C reaction, (the single and double escape peaks are also visible), and the 59.5 keV (0.06 MeV) gamma line emitted after the ^{241}Am decay.

4. Conclusions

In this work, we report a strong evidence of the fast neutron detection capability exhibited by a 2"×2" CLLB scintillation detector. Besides, we prove that it is possible to discriminate these fast neutron-induced events

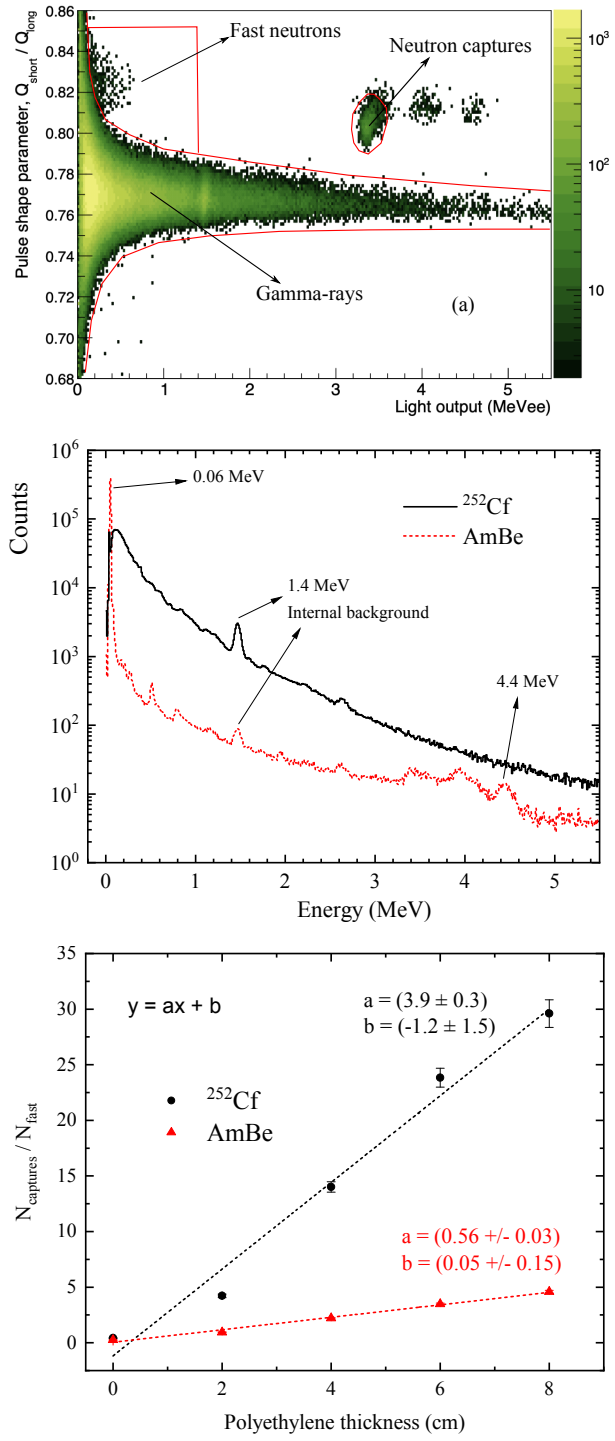

Figure 8: Ratio of neutron capture to fast neutron counts ($N_{captures}/N_{fast}$) as a function of the polyethylene thickness for ^{252}Cf and Am-Be neutron sources.

from the gamma-ray and thermal neutron events, by performing digital pulse shape discrimination analysis. We conduct measurements with an Am-Be source, unshielded and shielded, in order to study the response of the CLLB detector, to fast neutrons, gamma-rays and thermal neutrons, in single acquisition mode. In this case, we obtained a Figure of Merit $\sim$ 1.1 for fast neutron/gamma-ray discrimination.

Moreover, we conduct measurements in coincidence mode, both with a mono-energetic pulsed neutron source, at the Van de Graaff accelerator at the Legnaro National Laboratories (INFN-LNL, Legnaro-Italy), and with a continuous neutron spectrum (using a ^{252}Cf source). These coincidences measurements are needed to combine the PSD and ToF techniques to better discriminate the contributions of fast neutrons and gamma-rays. We are able to demonstrate the fast neutron detection capability of the CLLB detector. Combining the experimental results (in coincidence mode) and the the Monte Carlo simulation (GEANT4) results, it is possible to explain the mechanism of the the fast neutrons detection capability, i.e. the elastic scattering with ^{7}Li nuclei. Besides, the light output function of ^{7}Li ions in the CLLB crystal is determined. It is supposed that the light yield per unit of energy released by the ^{7}Li ions in the CLLB crystal is constant (dL/dE = κ). The best value obtained for κ is (0.36 $\pm$ 0.02).

Using this light output function, the intrinsic fast neutron detection efficiency is estimated by Monte Carlo simulation. It is obtained that for neutrons between 2 MeV and 10 MeV there is a slight variation of the efficiency (1.5-2%). Finally, as an application of these excellent results in the homeland security and nuclear safeguards fields, we report a method to rec-

ognize a neutron source using only the number of counts associated to fast neutrons and thermal neutron captures on ^{6}Li.

Acknowledgments

We thank the Van de Graaff accelerator staff for providing good quality pulsed beams. In particular, the support of L. Maran, is strongly acknowledged. This work was supported by the strategic project "INFN-ENERGIA" under the DRAGON experiment.

References

Al-Adili, A., Tarrío, D., Jansson, K., Rakopoulos, V., Solders, A., et al., 2020. Prompt fission neutron yields in thermal fission of U235 and spontaneous fission of Cf252. Phys. Rev. C 102, 064610. doi:10.1103/PhysRevC.102.064610.

Allison, J., Amako, K., Apostolakis, J., Arce, P., Asai, et al., 2016. Recent developments in Geant4. Nuclear Instruments and Methods in Physics Research Section A: Accelerators, Spectrometers, Detectors and Associated Equipment 835, 186–225. doi:10.1016/j.nima.2016.06.125.

Cazzaniga, C., Cremona, A., Nocente, M., Rebai, M., Rigamonti, et al., 2016. Light response of YAP:Ce and LaBr3:Ce scintillators to 4–30 MeV protons for applications to Telescope Proton Recoil neutron spectrometers. Nuclear Instruments and Methods in Physics Research Section A: Accelerators, Spectrometers, Detectors and Associated Equipment 820, 85–88. doi:10.1016/j.nima.2016.03.026.

Cester, D., Lunardon, M., Moretto, S., Nebbia, G., Pino, F., Sajo-Bohus, L., Stevanato, L., Bonesso, I., Turato, F., 2016. A novel detector assembly for detecting thermal neutrons, fast neutrons and gamma rays. Nuclear Instruments and Methods in Physics Research Section A: Accelerators, Spectrometers, Detectors and Associated Equipment 830, 191–196. doi:10.1016/j.nima.2016.05.079.

Cester, D., Nebbia, G., Stevanato, L., Pino, F., Sajo-Bohus, L., Viesti, G., 2013. A compact neutron–gamma spectrometer. Nuclear Instruments and Methods in Physics Research Section A: Accelerators, Spectrometers, Detectors and Associated Equipment 719, 81–84. doi:10.1016/j.nima.2013.04.032.

Dell'Aquila, D., Sweany, S., Brown, K., Chajecki, Z., Lynch, et al., 2019. Non-linearity effects on the light-output calibration of light charged particles in CsI(Tl) scintillator crystals. Nuclear Instruments and Methods in Physics Research Section A: Accelerators, Spectrometers, Detectors and Associated Equipment 929, 162–172. doi:10.1016/j.nima.2019.03.065.

D'Olympia, N., Chowdhury, P., Jackson, E., Lister, C., 2014. Fast neutron response of 6Li-depleted CLYC detectors up to 20 MeV. Nuclear Instruments and Methods in Physics Research Section A: Accelerators, Spectrometers, Detectors and Associated Equipment 763, 433–441. doi:10.1016/j.nima.2014.06.074.

Ferrulli, F., Labalme, M., Silari, M., 2022. Investigation of CLYC-6 for thermal neutron detection and CLYC-7 for fast neutron spectrometry. Nuclear Instruments and Methods in Physics Research Section A: Accelera-

tors, Spectrometers, Detectors and Associated Equipment 1029, 166460. doi:10.1016/j.nima.2022.166460.

Fontana, C., Tuccori, N., Pino, F., Lunardon, M., Stevanato, L., Moretto, S., 2020. Performance comparison between signal digitizers and low-cost digital oscilloscopes: Spectroscopic, pulse shape discrimination and timing capabilities for nuclear detectors. J. Inst. 15, P06020–P06020. doi:10.1088/1748-0221/15/06/P06020.

Fontana, C.L., Carnera, A., Lunardon, M., Pino, F.E., Sada, C., Soramel, F., Stevanato, L., Moretto, S., 2018. A distributed data acquisition system for nuclear detectors. Int. J. Mod. Phys. Conf. Ser. 48, 1860118. doi:10.1142/S2010194518601187.

Fontana, C.L., Lunardon, M., Pino, F.E., Stevanato, L., Carnera, A., Sada, C., Soramel, F., Moretto, S., 2017. A distributed data acquisition system for signal digitizers with on-line analysis capabilities, in: 2017 IEEE Nuclear Science Symposium and Medical Imaging Conference (NSS/MIC), IEEE, Atlanta, GA. pp. 1–5. doi:10.1109/NSSMIC.2017.8533063.

Giaz, A., Blasi, N., Boiano, C., Brambilla, S., Camera, F., Cattadori, C., Ceruti, S., Gramegna, F., Marchi, T., Mattei, I., Mentana, A., Million, B., Pellegri, L., Rebai, M., Riboldi, S., Salamida, F., Tardocchi, M., 2016a. Fast neutron measurements with 7Li and 6Li enriched CLYC scintillators. Nuclear Instruments and Methods in Physics Research Section A: Accelerators, Spectrometers, Detectors and Associated Equipment 825, 51–61. doi:10.1016/j.nima.2016.03.090.

Giaz, A., Pellegri, L., Camera, F., Blasi, N., Brambilla, S., Ceruti, S., Million, B., Riboldi, S., Cazzaniga, C., Gorini, G., Nocente, M., Pietropaolo, A., Pillon, M., Rebai, M., Tardocchi, M., 2016b. The CLYC-6 and CLYC-7 response to γ-rays, fast and thermal neutrons. Nuclear Instruments and Methods in Physics Research Section A: Accelerators, Spectrometers, Detectors and Associated Equipment 810, 132–139. doi:10.1016/j.nima.2015.11.119.

Hawrami, R., Pandian, L.S., Ariesanti, E., Glodo, J., Finkelstein, J., Tower, J., Shah, K., 2016. Crystals for Nuclear Security Applications. IEEE Trans. Nucl. Sci. 63, 509–512. doi:10.1109/TNS.2016.2522188.

Hull, G., Camera, F., Colombi, G., Josselin, M., Million, B., Blasi, N., 2019. Detection properties and internal activity of newly developed La-containing scintillator crystals. Nuclear Instruments and Methods in Physics Research Section A: Accelerators, Spectrometers, Detectors and Associated Equipment 925, 70–75. doi:10.1016/j.nima.2019.01.094.

Liang, F., Smith, J., 2020. Characterization of CLLBC Coupled to Silicon Photomultipliers. IEEE Trans. Nucl. Sci. 67, 927–932. doi:10.1109/TNS.2020.2988555.

Martínez-Dávalos, A., Belmont-Moreno, E., Michaelian, K., Menchaca-Rocha, A., 1997. Light-output response of CsI(Tl) detectors for low-energy ions. Journal of Luminescence 72–74, 769–771. doi:10.1016/S0022-2313(96)00313-4.

Mentana, A., Camera, F., Giaz, A., Blasi, N., Brambilla, S., Ceruti, S.,

Gini, L., Groppi, F., Manenti, S., Million, B., Riboldi, S., 2016. Measurement of fast neutron detection efficiency with ^{6} Li and ^{7} Li enriched CLYC scintillators. J. Phys.: Conf. Ser. 763, 012006. doi:10.1088/1742-6596/763/1/012006.

Mesick, K., Coupland, D., Stonehill, L., 2017. Pulse-shape discrimination and energy quenching of alpha particles in Cs 2 LiLaBr 6 :Ce 3+. Nuclear Instruments and Methods in Physics Research Section A: Accelerators, Spectrometers, Detectors and Associated Equipment 841, 139–143. doi:10.1016/j.nima.2016.10.033.

Pérez-Loureiro, D., Kamaev, O., Bentoumi, G., Li, L., Jewett, C., Thompson, M., 2021. Evaluation of CLYC-6 and CLYC-7 scintillators for detection of nuclear materials. Nuclear Instruments and Methods in Physics Research Section A: Accelerators, Spectrometers, Detectors and Associated Equipment 1012, 165622. doi:10.1016/j.nima.2021.165622.

Pino, F., Fontana, C., Delgado, J., Fabris, D., Nebbia, et al., 2021. Characterization of a medium-sized CLLB scintillator: Single neutron/gamma detector for radiation monitoring. J. Inst. 16, P11034. doi:10.1088/1748-0221/16/11/P11034.

Pino, F., Stevanato, L., Cester, D., Nebbia, G., Sajo-Bohus, L., Viesti, G., 2014. Detecting fast and thermal neutrons with a boron loaded liquid scintillator, EJ-339A. Applied Radiation and Isotopes 92, 6–11. doi:10.1016/j.apradiso.2014.05.025.

Qin, J., Xiao, J., Zhu, T., Lu, X., Han, Z., Wang, M., Jiang, L., Mou,

Y., Sun, J., Wen, Z., Wang, X., 2018. Characteristic of a Cs 2 LiLaBr 6 :Ce scintillator detector and the responses for fast neutrons. Nuclear Instruments and Methods in Physics Research Section A: Accelerators, Spectrometers, Detectors and Associated Equipment 905, 112–118. doi:10.1016/j.nima.2018.05.006.

Shirwadkar, U., Glodo, J., van Loef, E.V., Hawrami, R., Mukhopadhyay, S., Churilov, A., Higgins, W.M., Shah, K.S., 2011. Scintillation properties of Cs2LiLaBr6 (CLLB) crystals with varying Ce3+ concentration. Nuclear Instruments and Methods in Physics Research Section A: Accelerators, Spectrometers, Detectors and Associated Equipment 652, 268–270. doi:10.1016/j.nima.2010.08.050.

Shirwadkar, U., Gueorguiev, A., van Loef, E.V., Markosyan, G., Glodo, J., Tower, J., Shah, K.S., Pozzi, S., Clarke, S., Bourne, M., 2017. Multi-Signature Composite Detector System for Nuclear Nonproliferation, in: 2017 IEEE Nuclear Science Symposium and Medical Imaging Conference (NSS/MIC), IEEE, Atlanta, GA. pp. 1–4. doi:10.1109/NSSMIC.2017.8532812.

Smith, M., McClish, M., Achtzehn, T., Andrews, H., Baginski, M., Best, D., Budden, B., Clifford, E., Dallmann, N., Dathy, C., Frank, J., Graham, S., Ing, H., Stonehill, L., 2013. Assessment of photon detectors for a handheld gamma-ray and neutron spectrometer using Cs2LiYCl6:Ce (CLYC) scintillator. Nuclear Instruments and Methods in Physics Research Section A: Accelerators, Spectrometers, Detectors and Associated Equipment 715, 92–97. doi:10.1016/j.nima.2013.03.023.

Woolf, R.S., Phlips, B.F., Wulf, E.A., 2016. Characterization of the internal background for thermal and fast neutron detection with CLLB. Nuclear Instruments and Methods in Physics Research Section A: Accelerators, Spectrometers, Detectors and Associated Equipment 838, 147–153. doi:10.1016/j.nima.2016.09.013.